HHS Public Access

Author manuscript

Ann Surg Oncol. Author manuscript; available in PMC 2020 September 01.

Published in final edited form as:

Ann Surg Oncol. 2019 September ; 26(9): 2821–2830. doi:10.1245/s10434-019-07508-3.

Mathematical Modeling of the Metastatic Colorectal Cancer Microenvironment Defines the Importance of Cytotoxic Lymphocyte Infiltration and Presence of PD-L1 on Antigen Presenting Cells

Jenny Lazarus, MD[1], **Morgan D. Oneka, BS**[6], **Souptik Barua, MS**[6], **Tomasz Maj, PhD**[1], **Mirna Perusina Lanfranca, PhD**[1], **Lawrence Delrosario, MD**[1], **Lei Sun, PhD**[1], **J. Joshua Smith, MD, PhD**[2], **Michael I. D'Angelica, MD**[2], **Jinru Shia, MD**[3], **Jiayun M Fang, MD**[4], **Jiaqi Shi, MD, PhD**[4], **Marina Pasca Di Magliano, PhD**[1], **Weiping Zou, MD, PhD**[1], **Arvind Rao, PhD**[5,6,7], **Timothy L. Frankel, MD**[1]

[1] Department of Surgery, University of Michigan, Ann Arbor, MI

[2] Department of Surgery, Memorial Sloan Kettering Cancer Center, New York, NY

[3] Department of Pathology, Memorial Sloan Kettering Cancer Center, New York, NY

[4] Department of Pathology, University of Michigan, Ann Arbor, MI

[5]Department of Computational Medicine and Bioinformatics, University of Michigan, Ann Arbor, MI

[6]Department of Radiation Oncology, University of Michigan, Ann Arbor, MI

[7]Department of Biomedical Engineering, University of Michigan, Ann Arbor, MI

Abstract

Background—Although immune-based therapy has proven efficacious for some patients with microsatellite instability (MSI) colon cancers, a majority of patients receive limited benefit. Conversely, select patients with microsatellite stable (MSS) tumors respond to checkpoint blockade, necessitating novel ways to study the immune tumor microenvironment (TME). We used phenotypic and spatial data from infiltrating immune and tumor cells to model cellular mixing to predict disease specific outcomes in patients with colorectal liver metastases.

Methods—Formalin fixed paraffin embedded metastatic colon cancer tissue from 195 patients were subjected to multiplex immunohistochemistry (mfIHC). After phenotyping, the G-function was calculated for each patient and cell type. Data was correlated with clinical outcomes and survival.

Corresponding Author: Timothy L. Frankel, MD timofran@med.umich.edu Tel: 734-615-1269.

Results—High tumor cell to cytotoxic T lymphocyte (TC-CTL) mixing was associated with both a pro-inflammatory and immunosuppressive TME characterized by increased CTL infiltration and PD-L1$^+$ expression, respectively. Presence and engagement of antigen presenting cells (APC) and helper T cells (Th) were associated with greater TC-CTL mixing and improved 5-year disease specific survival compared to patients with a low degree of mixing (42% vs. 16%, p=0.0275). Comparison of measured mixing to a calculated theoretical random mixing revealed that PD-L1 expression on APCs resulted in an environment where CTLs were non-randomly associated with TCs, highlighting their biologic significance.

Conclusion—Evaluation of immune interactions within the TME of metastatic colon cancer using mfIHC in combination with mathematical modeling characterized cellular mixing of TCs and CTLs, providing a novel strategy to better predict clinical outcomes while identifying potential candidates for immune based therapies.

Synopsis

Mathematical modeling of phenotypic and spatial data of infiltrating immune cells illustrates the importance of cytotoxic lymphocyte and tumor cell mixing in colorectal liver metastases. By comparing differences between measured cellular mixing to a calculated random distribution of cells, the biologic consequence of immunosuppressive PD-L1$^+$ antigen presenting cells is observed.

Introduction

Colorectal cancer (CRC) is the third most common cancer in the United States and although treatable when discovered early, 21% of patients present with metastatic disease and have a 5-year survival rate of only 14 %[1]. The mainstay of therapy for patients with Stage IV disease is cytotoxic chemotherapy with occasional surgical metastasectomy in selected patients[2]. Recent advances in immune based therapies have changed the management of metastatic CRC in a small subset of patients resulting in durable disease control and in some cases, cure.[3]

In a majority of patients, the initiating events which trigger malignant transformation in the colon center around constitutive activation of a set of oncogenes (ie *KRAS* and *BRAF*) or repression of tumor suppressor genes (TP53)[2]. In roughly 15% of patients, CRC does not arise from a limited number of mutations but a broad perturbation of DNA repair mechanisms leading to numerous errors in genetic code. Characterized by the presence of repeated short segments of DNA called microsatellites, tumors displaying microsatellite instability (MSI) often lack mutations in the common oncogenes and tumor suppressors when compared to those with microsatellite stability (MSS). Arising either sporadically or associated with hereditary conditions, tumors from MSI patients are more likely to arise from the right colon, occur in younger patients and are associated with better survival[4,5]. The immune signatures of MSI tumors are unique and characterized by increased infiltration of pro-inflammatory cytotoxic T cells (CTLs) which likely contribute to a more favorable prognosis[6–8].

The cause of MSI is typically a defect in DNA damage repair machinery leaving cells with many errors in their genetic code. When DNA mutations occur, proteins produced from the altered genetic code are aberrant and are often recognized by the body as foreign. These "neoantigens"[4], are thought to be partly responsible for the increase in cytotoxic T cells (CTLs) present in the tumor microenvironment of MSI patients as the body attempts to rid itself of a foreign entity[6–9]. The degree of CTL infiltration is directly proportional to the number of DNA mutations present and therefore the neoantigen burden[4]. In addition to increased CTLs, present in the TME of MSI tumors is a compensatory immunosuppressive element characterized by increased programmed death receptor ligand 1 (PD-L1), an immune checkpoint, on both tumor cells (TC) and antigen presenting cells (APCs)[10–14]. Thought to be related to CTL infiltration and high PD-L1 expression, treatment of MSI high patients with checkpoint inhibitors against PD-1 has shown efficacy[15]. Interestingly, a small subset of MSS patients treated with checkpoint inhibitors in initial trials showed disease control with improvement in progression free survival[16]. Conversely, approximately 20% of MSI patients failed to show any benefit from treatment, highlighting a need to better understand details of the immune microenvironment. Work comparing the immune infiltration of CRCs has revealed subsets of MSS tumors which exhibit high CTL infiltration and the immunosuppressive elements often seen in MSI tumors suggesting a potential additional group that could benefit from immune based therapies[14].

Immune cell interaction in the TME is complex and not fully understood, highlighting the need for a method of analysis to yield more information and to increase efficacy of personalized cancer therapies. Recent data has demonstrated the capabilities of multiplex fluorescent immunohistochemistry (mfIHC) to both phenotype immune cells and provide spatial context, allowing for measurement of cell-to-cell interactions in the microenvironment and correlate those interactions with patient outcomes[14,17–19]. While prior work has considered interactions on a single cell level, a broader overview of the spatial patterns and general mixing of cells in the TME remains inadequate. We set out to use phenotypic and spatial data gathered from mfIHC to mathematically model the TME of CRC liver metastases to determine impact of cellular distribution on survival and thus better describe the role of PD-L1 positive APCs.

Methods

Patient Sample Collection

The study involving patient samples was approved by the institutional review board of Memorial Sloan Kettering, New York, NY. A collection of patient characteristics and survival data on 195 patients who underwent curative intent resection of colorectal liver metastasis was securely maintained. A pathologist reviewed whole tissue samples and selected 0.6mm diameter cores from each patient block in triplicate to create a tissue microarray (TMA). The patients in this data set who received preoperative chemotherapy received the standard chemotherapy treatment [20] and no patients received immunotherapy. Adjuvant chemotherapy regimens were not routinely recorded.

Multiplex fluorescent immunohistochemistry Staining and Imaging

Tumor microarray blocks were cut and placed onto charged slides for further processing. Slides were baked at 60 °C for one hour in a hybridization chamber and underwent deparaffinization and rehydration followed by staining as previously described[14]. Briefly, after rehydration, TMA slides were fixed with formalin and then subjected to the first round of antigen retrieval in antigen retrieval buffer with pH 9 (AR9, Akoya Biosciences). Six rounds of staining separated by antigen retrieval steps using either antigen retrieval buffer with pH 6 or pH 9 (AR6 and AR9, Akoya Biosciences) were completed on the slides resulting in a multiplex. Each antigen retrieval was followed by a primary and secondary antibody and fluorescent tyramide signal amplification (TSA, Akoya Biosciences). The following primary antibodies were used - CD3, CD8, CD163, PD-L1, pancytokeratin, and FOXP3 - followed by secondary antibody application (Opal polymer, Akoya Biosciences) and TSA. Spectral (DAPI) 4′,6-diamidino-2-phenylindole was used as a counter stain as previously described[14]. After slides were mounted, coverslipped and left to dry overnight, cores were imaged using the Mantra Quantitative Pathology Work Station (Akoya Biosciences) at 20x magnification in all channels: DAPI, FITC, CY3, CY5, CY7, Texas Red, Qdot with an exposure of 250msec. Each channel image was automatically merged into one image for further analysis.

Image Analysis: Phenotyping and cell-to-cell interactions

Simple and complex phenotyping as well as cell-to-cell interactions was performed using inForm software (Akoya Biosciences) and novel R based programs as previously described[14]. Briefly, the following phenotypes were assigned: T cells, regulatory T cells (Treg), helper T cells (Th), tumor cells (TC), cytotoxic T cells (CTL), antigen presenting cells (APC). The nearest distance from one cell to another (nearest neighbor) was calculated as was cell-to-cell engagement as previously described[14].

Image Analysis: spatial G-function with AUC metric

A G-function was calculated to quantify the spatial relationship, and therefore potential interaction, between two or more types of cells in the TME. The G-function is a function of a distance ‘r’, and computes the probability that cells of a “reference” cell type, type ‘i’, have a cell of a “non- reference” cell type, type ‘j’, within ‘r’ μm. This can be defined mathematically as $G(r) = Prob(\rho(x_i,X_j) \leq r)$ where $\rho(x_i,X_j) = \min\{ |x_i - x_j |_2 : x_j \in X_j \}$[20]is the distance between a cell of type ‘i’ and the nearest cell of type ‘j’. Additionally, to correct for edge effects, we apply a Kaplan-Meier correction to the G-function. The Area Under the Curve (AUC) metric of the G-function was used to characterize the rate at which the G-function rises. The AUC is defined as the area beneath the G-function curve from 0 up to a certain radius, and thus will be larger for quickly rising curves. The G-function AUC has been shown to be prognostic of outcomes in non-small cell lung cancer (NSCLC)[17] and intraductal papillary mucinous neoplasms (IPMN)[18]. The AUC was calculated using a radius of 60 microns (120 pixels given an image resolution of 1 pixel = 0.5 microns).

Statistical Analysis

Statistical analyses were performed using JMP Pro 13.2.0 unless stated otherwise. Differences in intercellular distances and engagement were evaluated by two-sided analysis of variance. For data not normally distributed, non-parametric Wilcoxon rank sum was used. Categorical variables were analyzed with Fisher's exact test. $p \leq 0.05$ were considered significant and were adjusted for multiple testing using the Benjamini-Hochberg False Discovery Rate (FDR) procedure when necessary. For survival analysis, Kaplan-Meier plots were drawn and statistical differences determined by log-rank. Multivariate analysis of survival was performed using Cox regression for components that were statistically significant on univariate analysis and those previously associated with survival following resection of CRLM.

Results

G-function mathematically models cellular mixing in the colorectal tumor microenvironment

In order to evaluate the immune infiltration and interaction in the tumor microenvironment of colorectal liver metastasis, mfIHC was completed on TMAs of colorectal liver metastasis from patients who underwent curative intent resection. TMA cores were stained and imaged and composite images analyzed using inForm software as previously described[14]. G-function, a mathematical expression of cellular mixing was calculated for interactions of CTLs ($CD3^+CD8^+$) and tumor cells (TCs) ($Pancytokeratin^+$) from each patient by averaging cellular interactions from the three available cores. The rate of rise of the G-function line represents the degree of cellular mixing with a rapidly or slowly rising line indicative of high and low mixing, respectively. The area under the curve (AUC) metric of this G-function was used to compare differences in mixing at a consistent radius (60 microns) from individual cells. A high AUC therefore represents high CTL-TC mixing, while a low AUC will be referred to as low CTL-TC mixing. A representative example of cellular phenotyping, mapping and G-function calculation is displayed in Figure 1. In patients where CTLs (yellow in the composite image and red in the phenotype map) and TCs (white in the composite image and blue in the phenotype map) are frequently spatially associated with each other (Figure 1 a,b), the corresponding G-function reveals a rapid rise in slope creating a higher AUC (Figure 1c). Conversely, when cells are present but rarely interact with each other (Figure 1d,e), the G-function displays a slowly rising curve and the AUC is lower (Figure 1f). Patients were divided into two groups - high cellular mixing of CTLs and TCs (high AUC based on the highest quartile AUCs) and low cellular mixing of CTLs and TCs (low AUC based on the lowest three-quarter AUCs) and corresponding patient demographics were gathered. Patients with a high AUC tended to be younger (56.8 yrs. vs. 61.9 yrs.; $p=0.0157$) and were more likely to be male (72% vs 28%; $p=0.154$). No significant correlation was found with type of surgical resection, prior liver resection, preoperative chemotherapy, extrahepatic disease, tumor diameter, tumor number, disease free interval or clinical risk score (Table 1).

High CTL-TC mixing was associated with both a pro-inflammatory and immunosuppressive microenvironment

High cellular CTL-TC mixing as defined by a high AUC was associated with increased infiltration of lymphocytes, macrophages and dendritic cells (Fig. 2a) and a high relative number of T cells (Fig. 2b) when compared to the low CTL-TC mixing group. Consistent with a more pro-inflammatory environment, tumors with a high CTL-TC AUC had a greater infiltration of CTLs in the TME (Fig. 2c), as well as a higher number of helper T cells (Th) (Fig. 2d). To further investigate the immunosuppressive elements of the tumor microenvironment (TME), tissue was stained for immunosuppressive regulatory T cells (Treg) ($CD3^+FOXP3^+$) as well as the checkpoint PD-L1 on TCs ($Pancytokeratin^+PD\text{-}L1^+$) and APCs ($CD163^+PD\text{-}L1^+$). While no difference was observed with respect to the relative frequency of Tregs (Fig. 2e), tumors with a high degree of CTL-TC mixing had elevated expression of PD-L1 on TCs (Fig. 2f). High AUC tumors displayed a greater infiltration of APCs (Fig. 2g) though these appeared to be a more immunosuppressive subtype as determined by elevated expression of $PD\text{-}L1^+$ (Fig. 2h). In summary, patient tumors with a high degree of CTL-TC mixing were associated with increased inflammation characterized by greater CTL infiltration as well as the high prevalence of the immunosuppressive checkpoint PD-L1 on both TCs and APCs.

High CTL-TC mixing was associated with improved survival and enhanced cooperation of APCs and Th cells

To examine the cooperation and/or priming of CTLs, we assessed associations between CTL-TC mixing and intercellular distances of CTLs to Th cells and APCs. The high CTL-TC mixing group was associated with a shorter Th cell to CTL distance suggesting a potential role in enhancement of CTL activity (Fig. 3a). APCs, which are also important mediators of cell priming through antigen presentation, were spatially associated with CTLs as demonstrated by shorter distance to nearest neighbor in the high AUC cohort (Fig. 3b). We have previously demonstrated that engagement, defined by proximity closer than one cell width, of Th cells and APCs with CTLs enhances the function of the latter[14]. This engagement was compared in the two cohorts of high and low mixing and we found significantly greater engagement of Th cell and APCs with CTLs in the more highly mixed cohort (Fig. 3c and 3d). To determine if this finding was specific to pro-inflammatory cells, we considered interactions of the immunosuppressive TME and investigated the association between high and low CTL-TC mixing and Treg-CTL engagement. Contrary to Th cells and APCs, the percentage of Tregs engaged to CTLs was not significantly different between the cohorts (Fig. 3e). To determine impact of mixing on survival, a Kaplan Meier curve was created comparing high and low G-function patients (Fig. 3g). The 5-year disease specific survival was higher in patients with a high degree of CTL-TC mixing (42%) when compared to the low mixing cohort (16%; $p=0.0275$). When considering extremes of survival, there were a statistically a greater number of early deaths (<2 years after surgery) in the low mixing group highlighting the importance of a robust pro-inflammatory infiltrate. Multivariate analysis including univariate differences as well as factors known to be associated with survival including tumor size and number was performed. In this model, only high CTL-TC AUC was associated with a statistically significant improvement in survival (HR 0.5901; $p=0.0126$).

PD-L1 expressed on APCs represses CTL-TC mixing

Due to the complex nature of the immune microenvironment, it can be difficult to establish the significance of a single cell subset on the entire population as a whole. Mathematical modeling allows one to describe multiple cellular interactions as a single entity, in this case TC-CTL mixing. For each patient, a random G-function was created representing the degree of mixing that could occur randomly from a fixed number of cells existing in the same relative space. Actual G-function curves were then compared to the random G-function curves and a delta G-function established for each patient. We considered any curve falling within one standard deviation of the random curve to represent random mixing (Figure 4a, Group B). Curves that fell greater than one standard deviation above the random curve represented non-random mixing (Group A) while those below one standard deviation represented non-random, non-mixing (Group C). Bivariate analysis revealed that the degree of non-random, non-mixing (negative delta G-function) was proportional to infiltration of PD-L1$^+$APCs (r^2=0.1722; $p<0.0001$) (Figure 4b). When comparing patients with and without PD-L1$^+$ APCs within their tumors, we find significantly more negative delta G-function AUCs in the former suggesting that they may inhibit CTL-TC interactions (Figure 4c). To confirm this, we separated patients into 3 cohorts based on their delta G-functions as above (Figure 4a). Only tumors which displayed non-random non-mixing had elevated PD-L1$^+$ APCs in the microenvironment when compared to the other cohorts (Figure 4d). Even more striking was that those PD-L1$^+$ APCs tended to be closer in distance and more engaged with CTLs in this immunosuppressive environment (Figure 4e,f). These data not only highlight the role of PD-L1$^+$ APCs in CRC TME, but also demonstrate to ability of this proposed methodology to model immune cell infiltration.

Discussion

Despite significant progress in the past three decades, metastatic CRC remains an often-fatal disease and is rarely cured. Evidence of efficacy of immune based therapies in a select subset of patients has brought attention to the need to better understand the immune microenvironment[3]. Describing complex immune-tumor cell interactions is important for determining prognosis as well as identifying patients who could benefit from immune based therapies. Previous studies have shown immune cell infiltration alone has a significant effect on disease specific survival[21–25]. For instance, it is well established that cytotoxic T cell infiltration is associated with a more favorable prognosis[19] and is associated with active anti-tumor immunity in the tumor microenvironment[10]. Identifying the presence of immune cells alone within a tumor gives an important view, albeit limited in biologic relevance. Identifying the interactions among tumor cells and immune cells enables a closer investigation of cellular activity and biological significance in the cancer microenvironment.

While much of the prior work has focused on simply identifying the types of cells in the TME[22,23,26], this ignores important spatial data which provides information regarding the context in which immune cells exist. mfIHC provides a new tool combining the multi-antigen phenotyping capability of flow cytometry with the in situ nature of traditional IHC.

Using this technique allows multiple cell types to be labeled and evaluated without disturbing the special arrangement of the cells. The ability to phenotype many more unique

cell types and capture spatial orientation data of each individual cell in a sample necessitates new bioinformatics approaches to process these large data sets. Mathematical modeling of the TME creates a platform to study complex interactions and determine the impact of single cell subtypes on the immune environment as a whole[17,18].

We performed mfIHC on a large dataset of patients undergoing hepatic resection for colorectal liver metastases. By focusing on patients undergoing curative intent resection, we attempted to identify a more homogenous metastatic cohort selecting patients with similar overall disease burdens (presumably little to no disease after resection).

While prior analysis of spatial features has been limited to interactions between two cell types, we employed modeling methodology which allowed us to capture the relationship between two populations as a whole. G-function is a measure of how tightly or loosely two cell populations intermix with one another[17]. Based on prior data that CTL to TC engagement was associated with immune activation and improved disease specific outcomes[14], we hypothesized that measurement of mixing would provide a more accurate representation of the TME and shed new light on complex interactions amongst other immune cells.

Patients were separated into those whose tumors showed a high or low amount of CTL-TC mixing based on their calculated G-function. Demographic data revealed that those with high mixing were more likely to be younger and male. This may reflect a greater number of MSI patients who tend to be younger men and whose tumors would be predicted to have highly engaged CTLs and therefore an elevated G-function. Importantly, there were no differences in tumor characteristics including the extent of operation and clinical risk score[27].

When examining features of the microenvironment, those with elevated G-functions had far more total immune cells (defined as all T cells and APCs) and pro-inflammatory CTLs and Th cells. While there was no difference in regulatory T-cell infiltration, the APCs that were present had upregulation of PD-L1, an immune checkpoint aimed at inhibiting the activity of CTLs. This is consistent with prior data demonstrating that, in response to enhanced inflammation, compensatory immune suppression is initiated[10,14]. It is likely that this scenario of heightened inflammation and reactive checkpoint expression represents the precise environment in which immune based therapies are most efficacious. To better determine if the PD-L1 bearing APCs were likely biologically active in the high CTL-TC mixed environment, we measured intercellular distances and found that PD-L1$^+$ APCs were closer and more engaged to CTLs. As predicted, in those with high mixing as determined by a high G-function, improved disease specific survival was seen.

With increasing data that PD-L1 expression on APCs significantly impacts the make-up of the TME, we next modeled their effects on CTL-TC mixing[14]. We determined that patients with PD-L1 expression on TCs or APCs had significantly lower G-functions indicating decreased cellular mixing. One issue with comparing G-functions in this setting is the interrelationship between total number of infiltrating cells and mixing. One can imagine that if many TCs or CTLs are present in the TME, by random chance, the likelihood of mixing is

higher than if one or both populations are infrequent. To account for this potential bias, we calculated a theoretical random G-function based on the number of cells present and then compared this to the calculated G-function. By doing so, we were able to show the biologic impact of PD-L1$^+$ APCs which resulted in decreased CTL-TC mixing in a non-random fashion.

Conclusion

Mathematical modeling of the metastatic CRC TME provides a more accurate description of cellular interactions. Increased mixing of TCs and CTLs, likely an indicator of antigen specific recognition/reactivity, is associated with improved survival and both an inflammatory and immune suppressive environment. Novel methods to interpret phenotypic and spatial data from the TME may better select patients for immune based therapies in the future.

Appendix/Acknowledgements

This work was supported by NIH K08CA201581(tlf) and K08CA234222 (js). M.O. was supported by T32 GM070449. A.R. and S.B were supported by CPRIT RP170719, CPRIT RP150578, NCI 1R37CA214955-01A1, a gift from Agilent Technologies, and a Research Scholar Grant from the American Cancer Society (RSG-16-005-1)

A. Rao is a member of Voxel Analytics, LLC, reports receiving other commercial research support from Agilent Technologies. J. Smith has received travel support for fellow education from Intuitive Surgical Inc. and has served as a clinical advisor for Guardant Health, Inc. All other authors have no relevant financial disclosures.

References

1. NIH. Surveillance, Epidemiology, and End Results Program. 2018.
2. Frankel TL, Vakiani E, Nathan H, et al. Mutation location on the RAS oncogene affects pathologic features and survival after resection of colorectal liver metastases. Cancer. 2017;123(4):568–575. [PubMed: 27737491]
3. Diaz LA Jr., Le DT. PD-1 Blockade in Tumors with Mismatch-Repair Deficiency. N Engl J Med. 2015;373(20):1979.
4. Deschoolmeester V, Baay M, Lardon F, Pauwels P, Peeters M. Immune Cells in Colorectal Cancer: Prognostic Relevance and Role of MSI. Cancer Microenvironment. 2011;4(3):377–392. [PubMed: 21618031]
5. Inderberg EM, Walchli S, Myhre MR, et al. T cell therapy targeting a public neoantigen in microsatellite instable colon cancer reduces in vivo tumor growth. Oncoimmunology. 2017;6(4):e1302631. [PubMed: 28507809]
6. Phillips SM, Banerjea A, Feakins R, Li SR, Bustin SA, Dorudi S. Tumour-infiltrating lymphocytes in colorectal cancer with microsatellite instability are activated and cytotoxic. Br J Surg. 2004;91(4): 469–475. [PubMed: 15048750]
7. Prall F, Duhrkop T, Weirich V, et al. Prognostic role of CD8+ tumor-infiltrating lymphocytes in stage III colorectal cancer with and without microsatellite instability. Hum Pathol. 2004;35(7):808–816. [PubMed: 15257543]
8. Guidoboni M, Gafa R, Viel A, et al. Microsatellite instability and high content of activated cytotoxic lymphocytes identify colon cancer patients with a favorable prognosis. Am J Pathol. 2001;159(1): 297–304. [PubMed: 11438476]
9. Schwitalle Y, Kloor M, Eiermann S, et al. Immune response against frameshift-induced neopeptides in HNPCC patients and healthy HNPCC mutation carriers. Gastroenterology. 2008;134(4):988–997. [PubMed: 18395080]

10. Llosa NJ, Cruise M, Tam A, et al. The vigorous immune microenvironment of microsatellite instable colon cancer is balanced by multiple counter-inhibitory checkpoints. Cancer Discov. 2015;5(1):43–51. [PubMed: 25358689]
11. Qu QX, Huang Q, Shen Y, Zhu YB, Zhang XG. The increase of circulating PD-L1-expressing CD68(+) macrophage in ovarian cancer. Tumour Biol. 2016;37(4):5031–5037. [PubMed: 26541760]
12. Lin H, Wei S, Hurt EM, et al. Host expression of PD-L1 determines efficacy of PD-L1 pathway blockade-mediated tumor regression. J Clin Invest. 2018;128(2):805–815. [PubMed: 29337305]
13. Curiel TJ, Wei S, Dong H, et al. Blockade of B7-H1 improves myeloid dendritic cell-mediated antitumor immunity. Nat Med. 2003;9(5):562–567. [PubMed: 12704383]
14. Lazarus J, Maj T, Smith JJ, et al. Spatial and phenotypic immune profiling of metastatic colon cancer. JCI Insight. 2018;3(22).
15. Arora SP, Mahalingam D. Immunotherapy in colorectal cancer: for the select few or all? J Gastrointest Oncol. 2018;9(1):170–179. [PubMed: 29564183]
16. Le DT, Uram JN, Wang H, et al. PD-1 Blockade in Tumors with Mismatch-Repair Deficiency. N Engl J Med. 2015;372(26):2509–2520. [PubMed: 26028255]
17. Barua S, Fang P, Sharma A, et al. Spatial interaction of tumor cells and regulatory T cells correlates with survival in non-small cell lung cancer. Lung Cancer. 2018;117:73–79. [PubMed: 29409671]
18. Barua S, Solis L, Parra ER, et al. A Functional Spatial Analysis Platform for Discovery of Immunological Interactions Predictive of Low-Grade to High-Grade Transition of Pancreatic Intraductal Papillary Mucinous Neoplasms. Cancer Inform. 2018;17:1176935118782880.
19. Carstens JL, Correa de Sampaio P, Yang D, et al. Spatial computation of intratumoral T cells correlates with survival of patients with pancreatic cancer. Nat Commun. 2017;8:15095. [PubMed: 28447602]
20. Andre T, Boni C, Mounedji-Boudiaf L, et al. Oxaliplatin, fluorouracil, and leucovorin as adjuvant treatment for colon cancer. N Engl J Med. 2004;350(23):2343–2351. [PubMed: 15175436]
21. Curiel TJ, Coukos G, Zou L, et al. Specific recruitment of regulatory T cells in ovarian carcinoma fosters immune privilege and predicts reduced survival. Nat Med. 2004;10(9):942–949. [PubMed: 15322536]
22. Katz SC, Bamboat ZM, Maker AV, et al. Regulatory T cell infiltration predicts outcome following resection of colorectal cancer liver metastases. Ann Surg Oncol. 2013;20(3):946–955. [PubMed: 23010736]
23. Katz SC, Pillarisetty V, Bamboat ZM, et al. T cell infiltrate predicts long-term survival following resection of colorectal cancer liver metastases. Ann Surg Oncol. 2009;16(9):2524–2530. [PubMed: 19568816]
24. Mahmoud SM, Paish EC, Powe DG, et al. Tumor-infiltrating CD8+ lymphocytes predict clinical outcome in breast cancer. J Clin Oncol. 2011;29(15):1949–1955. [PubMed: 21483002]
25. Winerdal ME, Marits P, Winerdal M, et al. FOXP3 and survival in urinary bladder cancer. BJU Int. 2011;108(10):1672–1678. [PubMed: 21244603]
26. Galon J, Costes A, Sanchez-Cabo F, et al. Type, density, and location of immune cells within human colorectal tumors predict clinical outcome. Science. 2006;313(5795):1960–1964. [PubMed: 17008531]
27. Fong Y, Fortner J, Sun RL, Brennan MF, Blumgart LH. Clinical score for predicting recurrence after hepatic resection for metastatic colorectal cancer: analysis of 1001 consecutive cases. Ann Surg. 1999;230(3):309–318; discussion 318–321. [PubMed: 10493478]

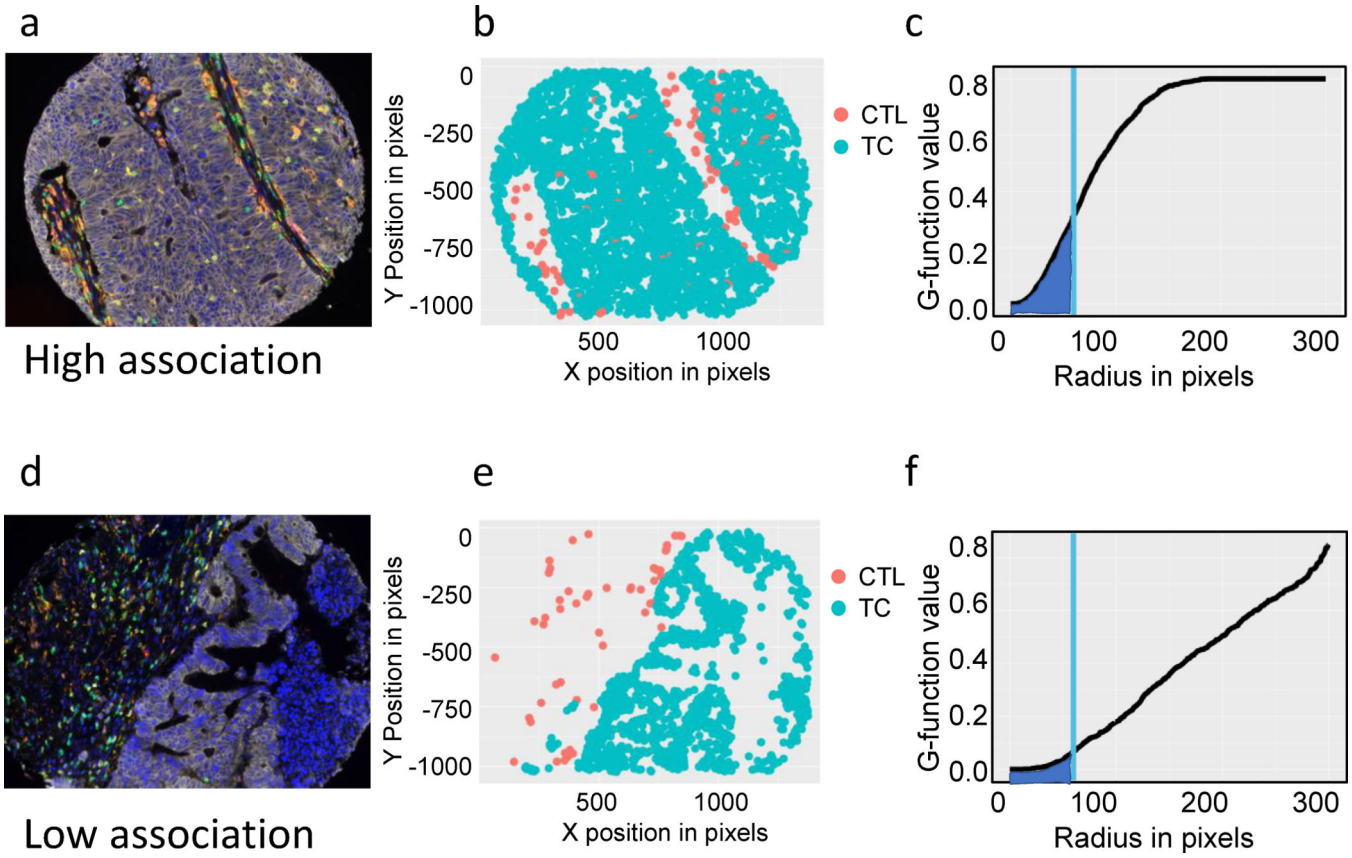

Figure 1: G-function mathematically models CTL-TC mixing

(1a) Multiplex fluorescent immunohistochemical composite image of a highly mixed CTL-TC tumor: TC (white), T cells (green), Tregs (green and red), CTLs (yellow), APCs (orange), PD-L1 (magenta), and DAPI (blue); **(1b)** spatial phenotype map of PDL1^{-}TCs (blue) and CTLs (red) provides two-dimensional cellular location; **(1c)** Spatial data is used to calculate the G-function (line), a mathematical representation of cellular mixing. Measurement of the area under the curve (AUC) at a fixed radius (blue) allows for comparisons of the rate of rise of the G-function. Representative example of a tumor with low CTL-TC mixing is shown **(1d-f)**.

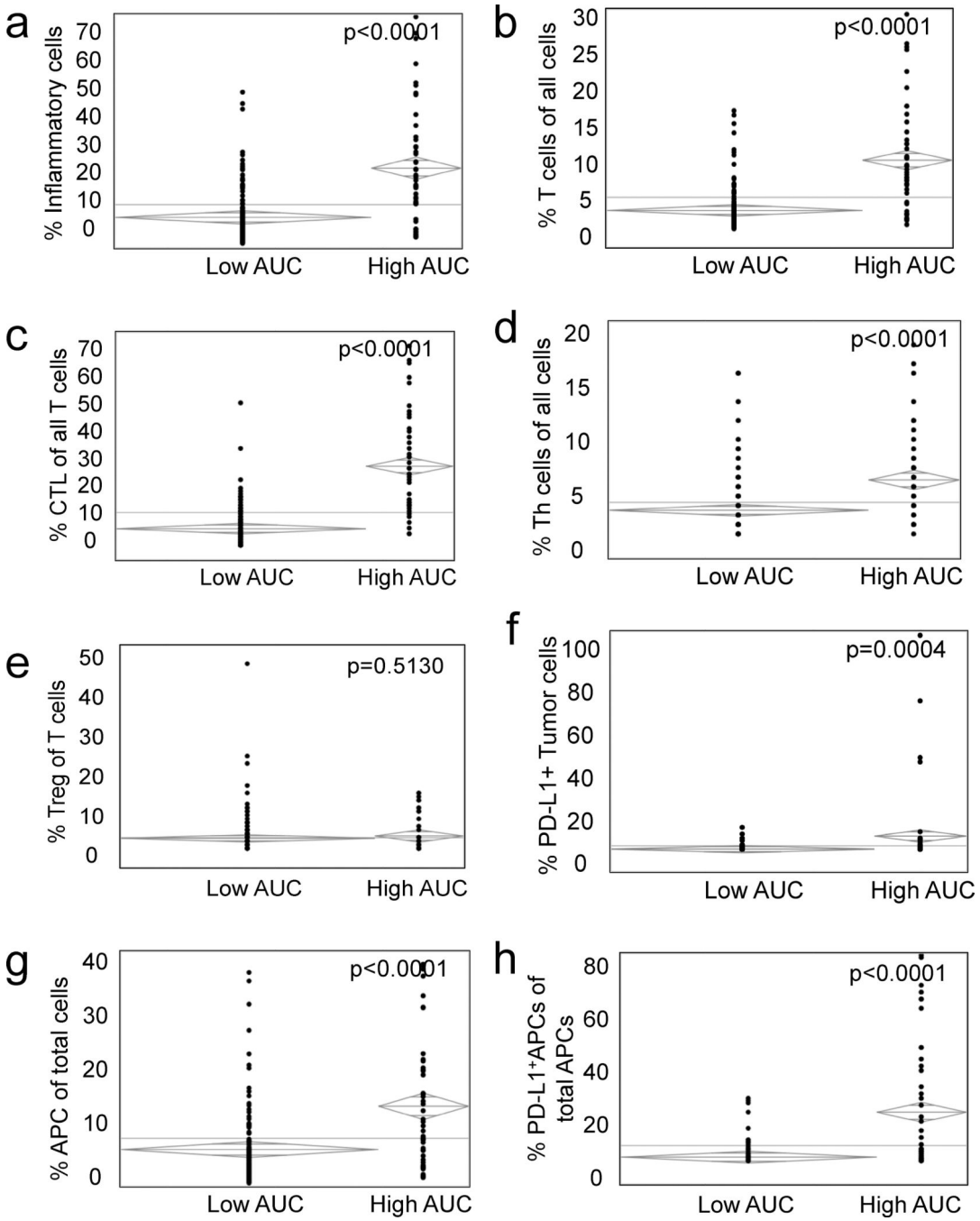

Figure 2: High CTL-TC mixing is associated with both a pro-inflammatory and immunosuppressive microenvironment.

Patients were separated into cohorts by G-function with high value patients representing tumors with elevated CTL-TC mixing and a low value, the converse. Relative to patients with low CTL-TC mixing, those with a high degree of cellular mixing tended to have a greater infiltration of inflammatory cells defined as lymphocytes, dendritic cells and APCs **(2a)** and a higher infiltration of T cells **(2b)** with a greater relative ratio of cytotoxic lymphocytes **(2c).** Other differences included a higher proportion of Th cells of total cells

(**2d)** while the relative amount of Tregs was similar (**2e)**. Analysis of checkpoint expression revealed a greater proportion of PD-L1+ TCs **(2f)** APCs **(2g,h)**.

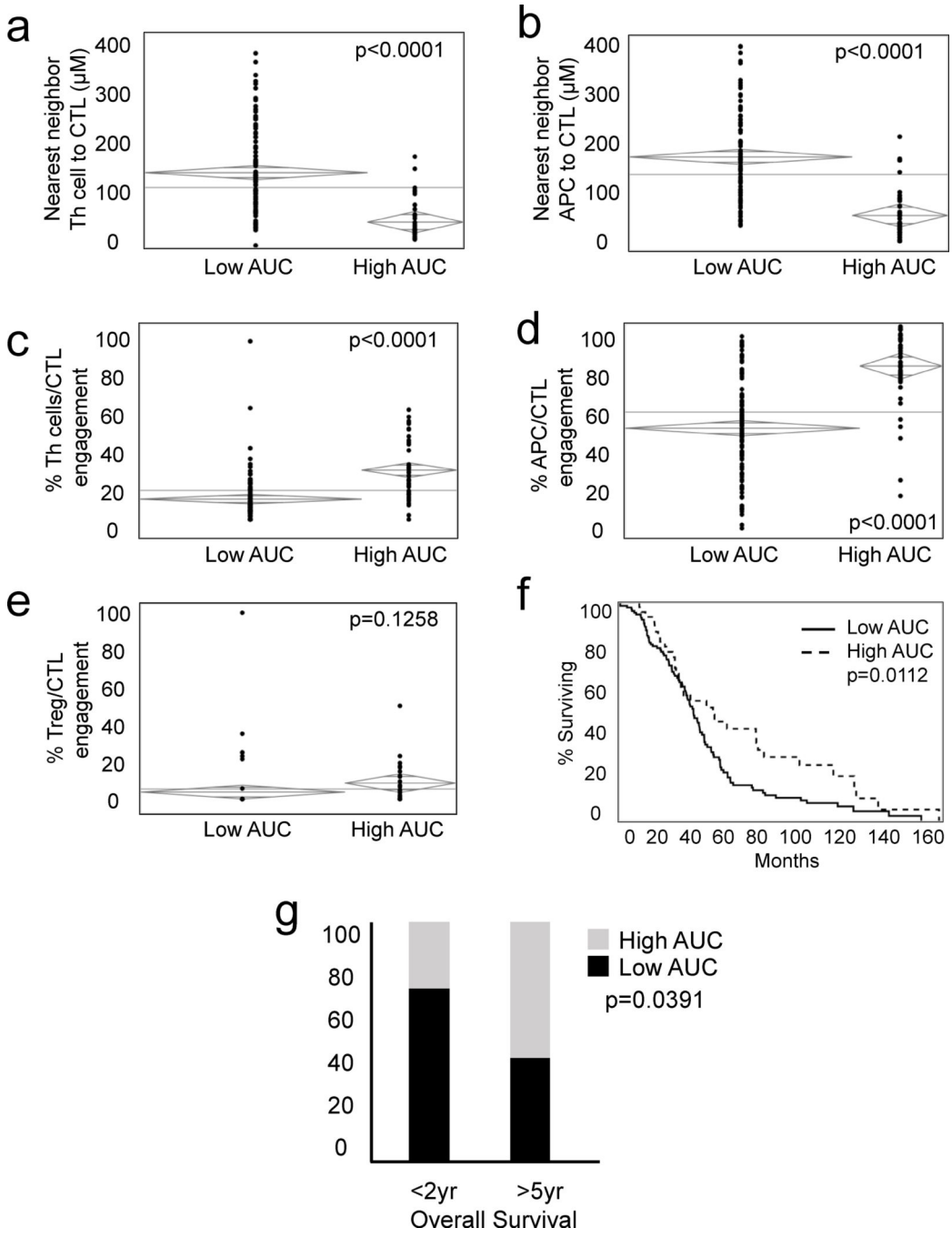

Figure 3: Modeling predicts immune cell engagement and survival following resection of metastatic colorectal liver metastases.

Patients with a high degree of CTL-TC mixing have decreased intercellular distances between CTLs relative to Th cells **(3a)** and APCs **(3b).** A similar trend was seen with engagement of CTLs with Th cells **(3c)** and APCs **(3d)** while no differences in CTL/Treg engagement was seen **(3e)**. Kaplan Meier curve **(3f)** identified improved survival in patients with high CTL-TC cellular mixing (high AUC) when compared to low CTL-TC cellular mixing (AUC). **(3g,h)**

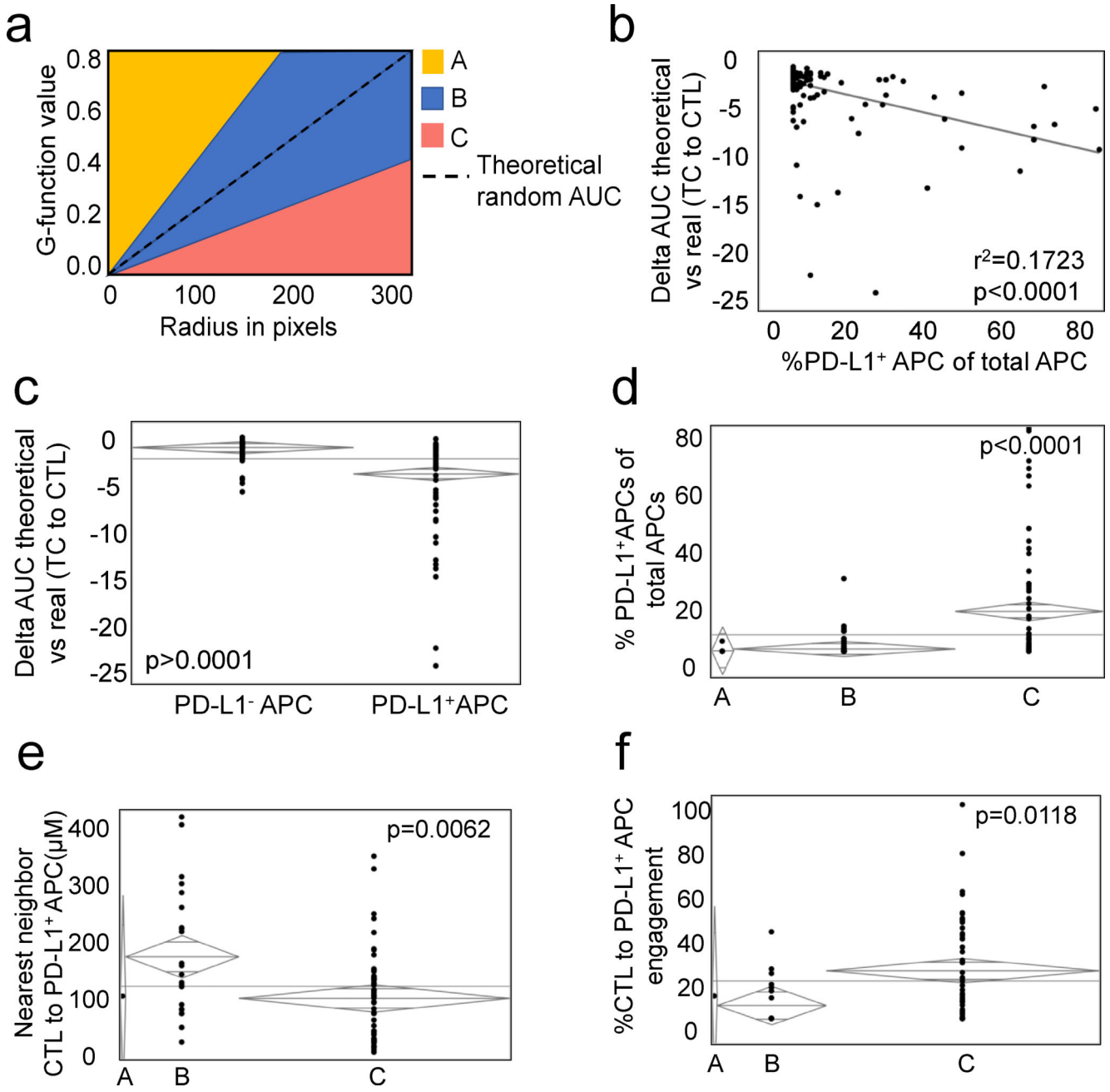

Figure 4: Differences between measured and predicted G-function highlight the importance of PD-L1$^+$ APCs in the TME.

(1a) A theoretical random G-function (dotted line) was calculated for each patient. Those with a measured G-function within one standard deviation of the theoretical random (blue shading, group B) were deemed to have a random degree for CTL-TC mixing. Those with a G-function one standard deviation greater than (shaded yellow, group A) or less than (shaded red, group C) the theoretical random were determined to have non-random CTL-TC mixing and non-random CTL-TC non-mixing, respectively. Bivariate analysis **(1b)** ANOVA **(1c)** revealed a close correlation between the delta theoretical random vs measured G-function AUC (dTvR) and ratio of PD-L1$^+$ APCs of total APCs. Examination of the

individual cohorts revealed a greater proportion PD-L1^{+} APCs in those with non-random CTL-TC non-mixing with associated decreased intercellular distance **(1e)** and engagement with CTLs **(1f)**.

Table 1:

Demographic and pathologic data of patients with high and low degrees of CTL-TC mixing.

Characteristic	High AUC n=46	Low AUC n=131	p-value
Mean age, yrs	56.8	61.9	0.0157
Gender			
Male	33 (72%)	66 (50%)	0.0154
Female	13 (28%)	65 (50%)	
Resection			
Wedge or segment	21 (46%)	56 (43%)	0.8854
Lobectomy	16 (20%)	45 (34%)	
Trisectionectomy	9 (34%)	30 (23%)	
Extra-hepatic disease			
Yes	5 (11%)	17 (13%)	0.2019
No	41 (89%)	114 (87%)	
Prior liver resection			
Yes	3 (7%)	9 (7%)	1.000
No	43 (94%)	122 (93%)	
Preoperative chemotherapy			
Yes	33 (79%)	82 (63%)	0.2867
No	13 (21%)	49 (37%)	
Mean preop CEA (95% CI)	134.9 (−146–416)	127.6 (−19–274)	0.9629
Mean largest tumor diameter, cm (95% CI)	4.3 (4.2–5.3)	4.8 (3.4–5.2)	0.4201
Tumor number			
1	28 (60%)	65 (50%)	0.2276
2	5 (11%)	29 (22%)	
3	5 (11%)	19 (15%)	
4	3 (7%)	8 (6%)	
5	0 (0%)	3 (2%)	
>5	5(11%)	7 (5%)	
Disease free interval, mos (95% CI)	16.0 (10.8–21.1)	18.4 (15.4–21.5)	0.4188
Clinical risk score			
1	20 (43%)	42 (32%)	0.9033
2	16 (35%)	54 (41%)	
3	7 (15%)	20 (15%)	
4	3 (7%)	14 (11%)	
5	0 (0%)	1 (1%)	